Journal of Ceramic Processing Research. Vol. 21, No. 1, pp. 123~130 (2020)
(Received 9 December 2019, Received in revised form 15 December 2019, Accepted 24 December 2019)
https://doi.org/10.36410/jcpr.2020.21.1.123

J O U R N A L O F
Ceramic Processing Research

Ruthenium(II) dicarboxylated bipyridyl based metal organic polymer as a sensitizer for nanostructured TiO_2 based dye-sensitized solar cells (DSSC)

Sathishkumar Chinnasamy and Sivasubramanian Ramanathan*
Electrochemical Energy Materials and Sensors Laboratory, NRIIC, PSG Institute of Advanced Studies, Coimbatore-4, Tamilnadu, India

In this work, ruthenium(II)bis(2,2'-bipyridyl4,4'-dicarboxylicacid)(pyrazine)bis(tetrafluroborate) [*Ru(II)(dcbpy)$_2$(pyz)]$_n$(BF$_4$)$_{2n}$*] based metal organic polymer *(RuMOP-Pyz-1)*, was synthesized at room temperature under inert atmosphere and their performance in dye-sensitized solar cells (DSSC) were studied. The metal organic polymer was prepared by coupling pyrazine as linker units with the Ru(II) dicarboxylated based mono metallic complex. The UV-visible absorption profiles covered a broad range of absorption and the formation of polymer leads to shift in the absorption wavelength. The metal mediated π-conjugation units in the polymer complex exhibit a strong emission at λ_{em} = 552 nm with an excitation wavelength of 395 nm. The synthesized metallo-polymer was employed as a sensitizer in DSSC and the maximum power conversion efficiency (PCE) value of η = 1.507 % with short circuit current (J_{sc}) of 3.22 mA/cm^2; open circuit voltage (V_{oc}) 0.684 V and Fill Factor (FF) of 68.45 % under Air Mass (AM) 1.5 G simulated sunlight at a light intensity of 100 mW/cm^2 was obtained. The efficiency of the device and its photovoltaic performances were found to be satisfactory. The enhanced performance of the device is attributed to the presence of extended conjugation of the metallo polymer which helps in a facile electron transfer from the HOMO to LUMO of TiO_2.

Keywords: DSSC, metallo-polymer, poly-Ru(II)dicarboxylated bipyridyl, pyrazine, photovoltaic, sensitizer.

Introduction

Dye sensitized solar cells (DSSC) are currently attracting significant attention as alternative to conventional silicon solar cells [1, 2] due to their low production cost, simplicity of fabrication, lightweight, array of colour and high power conversion efficiency (PCE). DSSC have been intensely pursued in last two decades and has found many applications such as flexible electronics, transparent conducting windows, etc. [3-5]. Typically DSSC is a multilayer device, where nanocrystalline titania coated on a conductive substrate act as a photoanode, platinized counter electrode act as a photocathode. The photoanode (TiO_2) with the dye and the photocathode electrode were bridged by a redox electrolyte, which mediates the charge transfer between the electrodes. The sensitization is usually a metal based organic dye which helps to improve the overall efficiency of DSSC [6, 7]. As being a multilayer device, the most important components of DSSC is the photosensitizer [8-10] and the efficiency of DSSC mainly depends on the performance of the sensitizers [11].

In view of the potential application of DSSC, more number of research works focused on each layer of DSSC like the photoanode, the photo cathode, the dyes and the electrolyte. In the case of photo anode, various nanostructured ceramics [12], semiconductor metal oxides with optimized layer deposition and sintering process [13] were examined. Further, in the case of photo cathode DSSC performances were enhanced by the addition of conducting ceramic nanoparticles [14] and microporous ceramics [15] in electrolyte systems. Specially, to increase the near-infrared solar cell response by introducing transparent ceramics [16] and to get excellent pigmenting materials through new ceramic dyes [17] has also been developed.

Predominantly, the ceramics based material for DSSC research were played a vital role in various approach. Particularly, by introducing TiO_2 nanowires, carbon nanofibers and porous carbon nanofibers with Pt catalysts were reported effective results [18-22]. Hence, ruthenium nanocrystals, composites based on TiO_2 nanoparticle/ nanowires, size-selected titanium dioxide nanowires, mixed transition metal oxides TiO_2 based photoanodes were also incorporated for efficient dye sensitized solar cells [23-27]. By introducing various synthetic designs in dye structure and blended structures of polymers [28] would increase the efficiencies of the solar cells. So, enhancing the DSSC performance by introducing new functional dyes is the focus of the current research [29]. Different types of dyes have been used in DSSC, including natural [30], organic [31, 32] and organometallic dyes [33] based on various transition elements [34].

*Corresponding author:
Tel : +422 434 4000
Fax: +422 257 3833
E-mail: rss@psgias.ac.in

Predominantly, ruthenium complexes have received intensive interest due to their favorable photo-electro-chemical properties and high stability. Among these sensitizers ruthenium polypyridyl based complexes have shown the best photovoltaic performance due their better light harvesting properties upon absorption [35]. In particular, the dicarboxylated bipyridine based mononuclear dyes N3 and N719 dye were considered as standard dyes due to their best photovoltaic performance [36, 37]. So far several DSSCs based on ruthenium complexes have achieved photovoltaic efficiencies of over 10% under standard measurement conditions and the highest value is about 12% [38, 39].

Recently, inorganic perovskite sensitized solid state DSSC have reached an efficiency of 20.1% [40]. On the other hand, the environmental and health hazards owing to the occurrence of toxic components hold back their commercial applications [41-43]. So, there is a high demand in the ruthenium based sensitizers which achieves high efficiency with proper electronic and structural properties [44]. In the case of standard sensitizers like N3 dye, the main drawback is the ambidentate thiocyanate ligand which will coordinate either at the nitrogen atom or at the sulfur atom. So as to solve the problems associated to NCS ligand based dyes, cyclo-metallated ruthenium complexes were projected in the last three decades [45]. An immense effort has been made to optimize the molecular structure of ruthenium complex by varying ancillary ligands, typically bipyridines which can be tuned by different substituent's to modify their photochemical and photophysical properties [46]. It has been well-accepted that raising the molar extinction coefficient of a sensitizer is a well-designed approach to enhance the photovoltaic performance [47].

Another important factor that hinders the performance of DSSC is the poor thermal stability [48]. To overcome this problem, supramolecular metallo-polymers with extended π-conjugation units were employed. These metallo-polymers exhibit the combination of both the properties of organic and organometallic compounds [49]. Moreover, these dyes show not only competent light harvesting efficiency but also an extended absorption with high molar absorption coefficient. Besides an effective intramolecular spatial charge separation of the excited state are critically important for better performance. Ruthenium based metallo-polymers which consists more number of conjugated units has various advantages, such as long-lived metal to ligand charge transfer (MLCT) and ligand centered redox process [50]. Employing the organic polymeric materials as sensitizers in DSSC has been recently recognized and comparatively modest research work done has been carried out [51]. In this work, we report the synthesis and characterization of ruthenium (II)bis(2,2'-bipyridyl4,4'-dicarboxylicacid) (pyrazine) bis(tetrafluroborate) based metal organic polymer ***(RuMOP-Pyz-1)*** and their efficacy as a photosensitizer is examined.

Experimental Section

Materials and methods

$RuCl_3.3H_2O$, 4,4'-dimethyl 2,2'-bipyridine (bpy) (<99%), 10% palladium on charcoal, Pyrazine (<99.5%), silver tetrafluroborate ($AgBF_4$) (<99%), P_{25} TiO_2 powder (<99%), $TiCl_4$ solution, chloro platinic acid (H_2PtCl_6), ethanol, N-methyl pyrrolidine (NMP), acetyl acetone and diethyl ether were purchased from Sigma Aldrich and were used as received. Triton X - 100 (<98%) were purchased from Merck and used as received. All the synthetic reactions were performed under inert condition. The solvents employed for the synthesis were reagent grade which were freshly distilled and degassed prior to use.

Characterization

The absorption spectra were recorded in DMF by using Shimadzu UV-1800 UV-VIS spectrophotometer (Japan) with 1 cm^2 quartz cell. Emission properties were studied by using Shimadzu RF-6000 spectrofluoro-photometer (Japan). FTIR spectra were assessed in the $400 \sim 4000\ cm^{-1}$ region by using IR Affinity FTIR, (Shimadzu, Japan). The AFM analysis was obtained by using NT-MDT (Ntegra Aura, NTMDT Co, Russia). FESEM analysis were taken by FESEM – (SIGMA HV – Carl Zeiss, Bruker Quantax 200 – Z10 EDS Detector). Raman analysis was performed by a micro Raman spectrometer (Horiba Jobin-LabRam-HR UV-vis μ-Raman spectrometer, Finland) at ambient temperature with Argon laser with an excitation wavelength of 514 nm equipped with CCD detector.

Synthesis

The metal organic polymer *(RuMOP-Pyz-1)* was synthesized by a one-pot reaction. The metal organic polymer was obtained by reacting the mono metallic complex with the linker unit as follows. 5 mL of dry ethanol solution of $Ru(dcbpy)_2Cl_2$ (0.0807 mmol), 5 mL of $AgBF_4$ (0.1613 mmol) in ethanol was added under argon atmosphere and stirred for 2 h at room temperature. The precipitated AgCl was filtered and to the obtained solution, 5 mL of pyrazine (0.0884 mmol) in ethanol was added drop wise and stirred for 1 h. The metallo-polymer was filtered, washed with ethanol (50 mL). Further purification was obtained by treating it with N-methyl pyrrolidine (NMP) and precipitating it with addition of diethyl ether. Finally, the precipitated metallo-polymer was dried under vacuum at 40 ºC for 8 h. The metal organic polymer *(RuMOP-Pyz-1)* was obtained as a dark red-brown solid (yield: 97%). The detailed synthetic pathway was illustrated in Scheme 1.

Analysis of $[Ru(II)(dcbpy)_2(pyrazine)]_n(BF_4)_{2n}]$ ***(RuMOP-Pyz-1)*****:** UV-Vis (3.5×10^{-5} M in Ethanol): λ_{max}/nm 535. Emission (λ_{max}) 553 nm excited at 395 nm. Melting Point: >450 ºC. FTIR (KBr disk) ν/cm^{-1}:

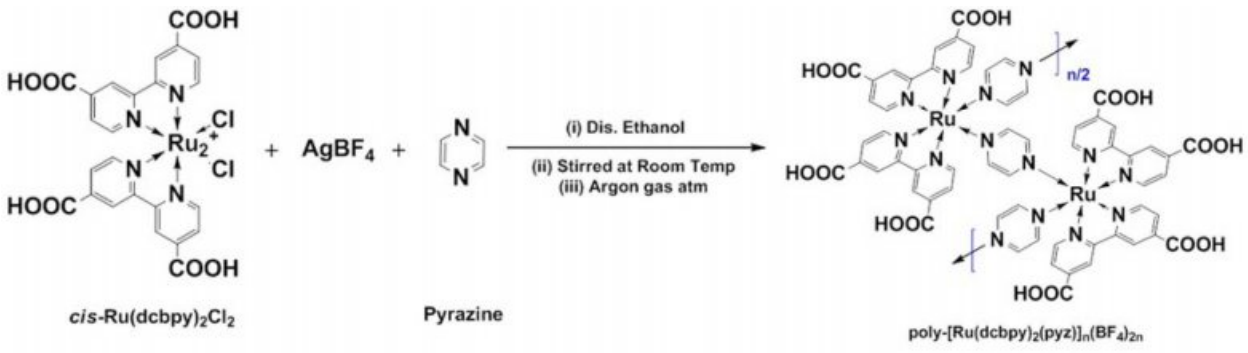

Scheme 1. Depicts the synthesis of poly-$[Ru(dcbpy)_2(pyz)]_n(BF_4)_{2n}$, coded as ***(RuMOP-Pyz-1)***, where (dcbpy) - 2,2'-bipyridyl 4,4'-dicarboxylic acid, (pyz) - pyrazine (linker unit), *cis*-$Ru(II)(dcbpy)_2Cl_2$ - *cis*-dichlorobis(2,2'-bipyridyl 4,4'-dicarboxylicacid)ruthenium(II) and poly-$Ru(dcbpy)_2(pyrazine)]_n(BF_4)_{2n}$ - poly [Ruthenium(II) bis(2,2'-bipyridyl4,4'-dicarboxylicacid) (pyrazine)bis tetrafluroborate)].

3452 (b), 2108 (m), 1984 (m), 1751 (s), 1630 (s), 1604 (s), 1513 (s), 1491 (s), 759 (s).

Fabrication of DSSC

Fluorine doped tin oxide glass (FTO) (~7 Ω/sq, purchased from Sigma Aldrich) plates were cleaned by ultrasonication with water, isopropanol and finally dried under nitrogen atmosphere. The cleaned substrate was heated up to 500 ºC for 25 min to remove organic contaminants and cooled down to room temperature. The compact layer of titania nanoparticle (pre treatment) was coated by immersing the FTO plates in a 40 mM aqueous $TiCl_4$ solution at 70 ºC for 30 min and followed by a series of sintering steps ((i) 325 ºC for 10 min, (ii) 375 ºC for 10 min, (iii) 450 ºC for 15 min, and (iv) 500 ºC for 30 min). Then by using mortar and pestle, P_{25} TiO_2 powder, acetyl acetone, Water and Triton X - 100 ingredients were grinded to paste. Then the prepared paste was coated on the pretreated (compact layer) FTO substrates by doctor-blade method and 12 µm thick film (active layer) was achieved. The TiO_2 pastes coated FTO plates were subjected to the above mentioned similar sintering steps. After cooling to room temperature, the TiO_2 electrodes were sensitized with metallo polymeric dye *(RuMOP-Pyz-1)* by immersing the electrode in 20 mM sensitizer solution in DMF. Similarly photocathode platinum coated FTO were prepared by using 0.005 M of H_2PtCl_6 solution. By using spray gun, the prepared solution was spread on cleaned pre-heated FTO plates at 50 ~ 60 °C. After the coating the slide was kept on hot plate at 380 °C. In air atmosphere the pretreated plates were kept in hot plate and the temperature of the hot plate was gradually increased from 100 °C to 380 °C. The plates were pre-annealed at 380 °C for 30 min and then slowly cooled down to 80 °C in air atmosphere. The coated plates can be used at any time, by giving the photocatalytic regeneration activity by pre annealing it on hot plate at 380 °C for 30 min.

Photovoltaic characterization

The current-voltage (I-V) characteristics were recorded by applying an external potential bias to the cell while recording the generated photocurrent with a Keithley model 2420 digital source meter. The light source was a 450W xenon lamp (Oriel) equipped with a Schott K113 Tempax sunlight filter (Praezisions Glas & optic GmbH) in order to match the emission spectrum of the lamp to the AM 1.5G standard. The metal organic polymer *(RuMOP-Pyz-1)* sensitized DSSC was tested under simulated AM1.5G illumination (power 100 mW cm^{-2}) using standard 1-Butyl 3-Methyl Imidazolium Iodide [BMII] electrolyte containing the iodine/tri iodide couple as the redox shuttle.

Results and Discussion

Synthesis of metal organic polymer dye *(RuMOP-Pyz-1)*

The synthesis of *RuMOP-Pyz-1* was prepared by the reaction of *cis*-dichlorobis(2,2'-bipyridine 4,4'-dicarboxylic acid) ruthenium (II), *cis*-$Ru(dcbpy)_2Cl_2$ with $AgBF_4$ (the chloride is removed by the precipitation of AgCl) and the metallo-polymer is formed by the reaction with pyrazine which acts a linker. It is found that the obtained metal organic polymer is soluble in polar aprotic solvent like DMF, DMSO, etc..

UV-Visible Spectroscopy

The UV-vis absorption spectrum of the metal organic polymer *(RuMOP-Pyz-1)* in DMF solutions were shown in the Fig. 1(a). The absorption spectrum shows a sharp band at 314 nm, which corresponds to the ligand π - π* transitions [52, 53]. A very broad and more intense band was obtained in the visible and near visible regions at 535 nm and 395 nm for the compound *RuMOP-Pyz-1* respectively. The bands in the visible and near visible region bands were assigned to metal-to-ligand charge transfer (MLCT) band of (d - π*) transition and π - π* transition of the conjugated linking units respectively. It is worth noting that compared with the other Ru(II) dicarboxylated based complexes, the synthesized metal organic polymer showed extended absorption beyond

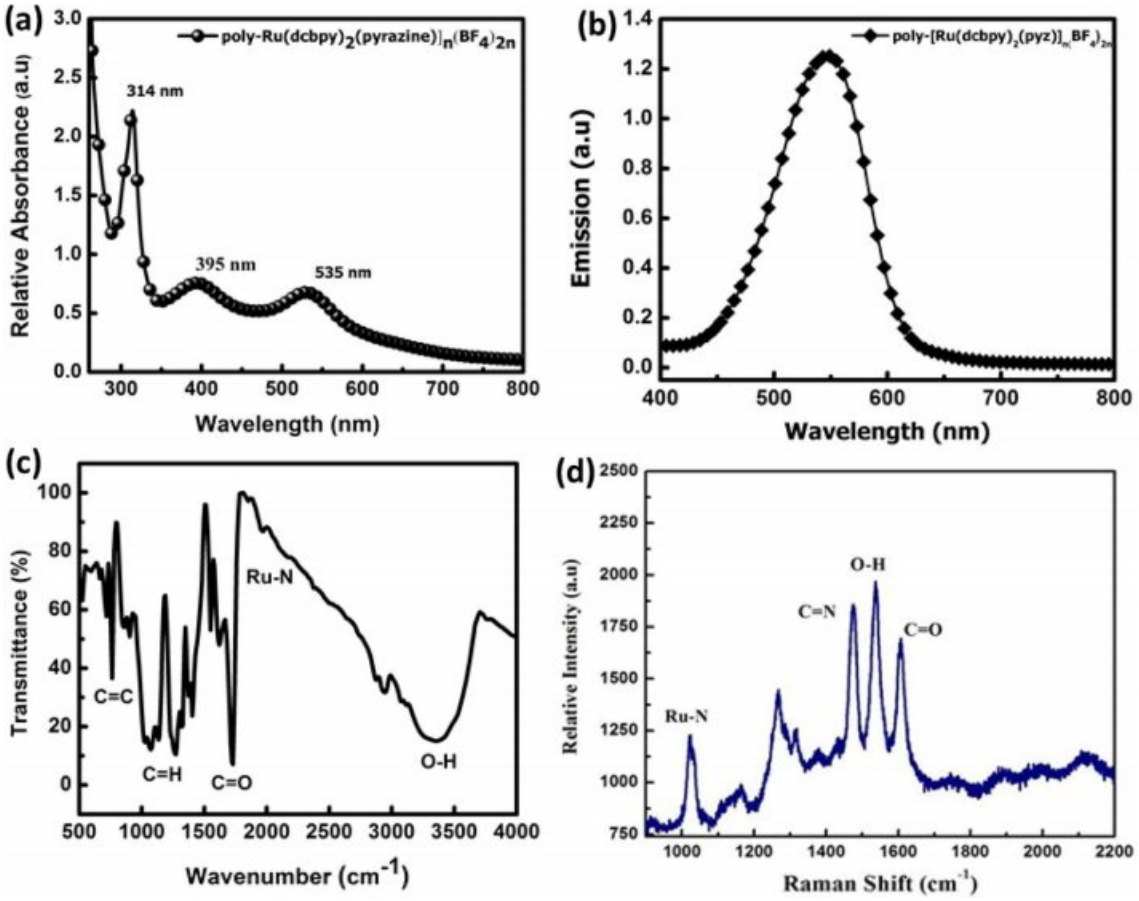

Fig. 1. (a) UV-Vis spectra of ***(RuMOP-Pyz-1)*** in DMF; (b) Emission spectrum ***(RuMOP-Pyz-1)*** in DMF; (c & d) FTIR and Raman Spectrum of ***(RuMOP-Pyz-1)*** respectively.

MLCT. The reason for this red shift could be due to the presence of extended conjugated systems with the electron withdrawing carboxylic acid groups, which lowers the energy of the π* orbital of the ligand [54].

Emission properties

The excitation of *RuMOP-Pyz-1* was carried out at 395 nm and the corresponding emission spectrum was obtained at 553 nm as shown in Fig. 1(b). This broad emission spectrum is due to the lower π* orbital of the 2,2'-bipyridyl-4,4'-dicarboxylic acid ligand and it is mainly due to the presence of electron-withdrawing substituent which is expected to give the longer lifetime. It has been noted that as the metal extended π-conjugation increases, a strong and broad phosphorescence spectrum was obtained [55].

FTIR and raman spectroscopy

The FTIR spectrum of *RuMOP-Pyz-1* in Fig. 1(c) showed a strong band in the region of 3,400 cm^{-1}, due to the presence of O-H group of the carboxylic acid moiety. The relatively strong absorption at 1,711 cm^{-1} corresponds to the stretching vibration mode of C=O bond and the bands at 1,362 cm^{-1} and 1,603 cm^{-1} are due to the symmetric and asymmetric stretching in the C=O and C-H bands respectively. Due to the N-coordination from the pyrazine unit a stretching vibrational modes at frequency of 2,011 cm^{-1} for the γ(Ru-N) band was obtained [56]. Furthermore, the C-C bond linkage in the aromatic skeleton was confirmed by the absorption peak at 804 cm^{-1}. The Raman spectrum in Fig. 1(d) was obtained for the ruthenium (II) dicarboxylated bipyridyl based metal organic polymeric dye *RuMOP-Pyz-1*, at an excitation wavelength of 430 nm. The vibration modes at 1,102 cm^{-1}, 1,471 cm^{-1}, 1,539 cm^{-1}, 1,610 cm^{-1} corresponds to Ru-N, C=N, O-H, C=O groups of the synthesized metal organic polymer respectively.

DSSC Fabrication – Electrode preparation

The typical DSSC and the detailed preparation involved in each layer of DSSC is as follows, as is given in the Scheme 2. The photo anode being the nanostructured TiO_2 sensitized with the metal organic polymer dye and photocathode being the Pt coated FTO and the cell was fabricated with BMII electrolyte as redox couple. With light irradiation, the sensitizer absorbs the dye and moves to excited state where by shuttling the electron to TiO_2 which in turn pass through the circuit to photocathode. Further the electrolyte helps in shuttling the electron from photocathode to

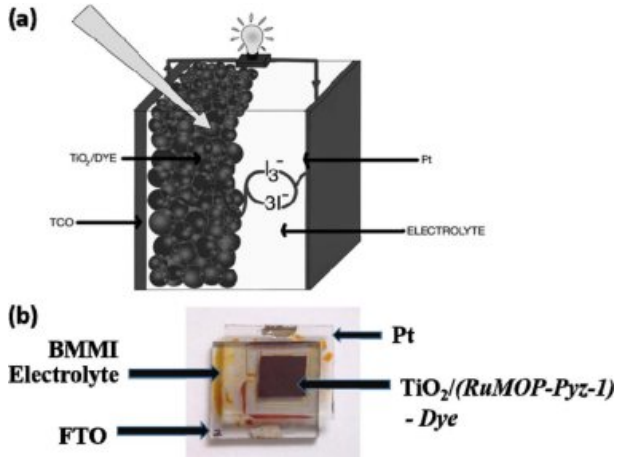

Scheme 2. (a) Schematic representation of typical DSSC device; (b) Real time DSSC device in which the sensitizer is ***(RuMOP-Pyz-1)*** (poly-ruthenium(II)bis(2,2'-bipyridyl4,4'-dicarboxylicacid)(pyrazine)bis(tetrafluroborate) - poly-$[Ru(dcbpy)_2(pyrazine)]_n(BF_4)_{2n}$).

dye. The overall efficiency of the device is deduced using the following equation,

$$\text{Efficiency } (\eta) = (V_{oc} * J_{sc})/(P) * FF \quad (1)$$

AFM and FESEM analysis

The AFM 2D images of the nanostructured coating of TiO_2 nanoparticles on FTO glass plate and its adsorption with the metal organic polymer dye *RuMOP-Pyz-1* were clearly seen from the Fig. 2. The surface topography of the FTO, compact layer, active layer and dye adsorption were shown in the Fig. 2(a, b, c & d) respectively. To determine the average pore size, ImageJ analysis software, were utilized and the average diameter of the pores in between the TiO_2 nanoparticles to be ~10 and ~30 nm for compact layer and active layer coating of TiO_2 nanoparticles . The root-mean-square roughness (RMS) values of the each layer were 70, 90, 170 and 650 nm. The increased value of RMS indicates that reduced amount reflectivity of incoming light confirms the formation of TiO_2 nanoparticles on FTO.

The FESEM image of the bare FTO, Compact layer and active layer coating of nanocrystalline titania on FTO were clearly shown in Fig. 3. The FTO deposition on glass substrate was shown in Fig. 3(a). The compact layer of deposition of titania nanoparticle as pretreatment for the photoanode as barrier layer on FTO was achieved (Fig. 3b) by dipping the FTO plates in a 40 mM aqueous $TiCl_4$ solution and followed by a series of sintering

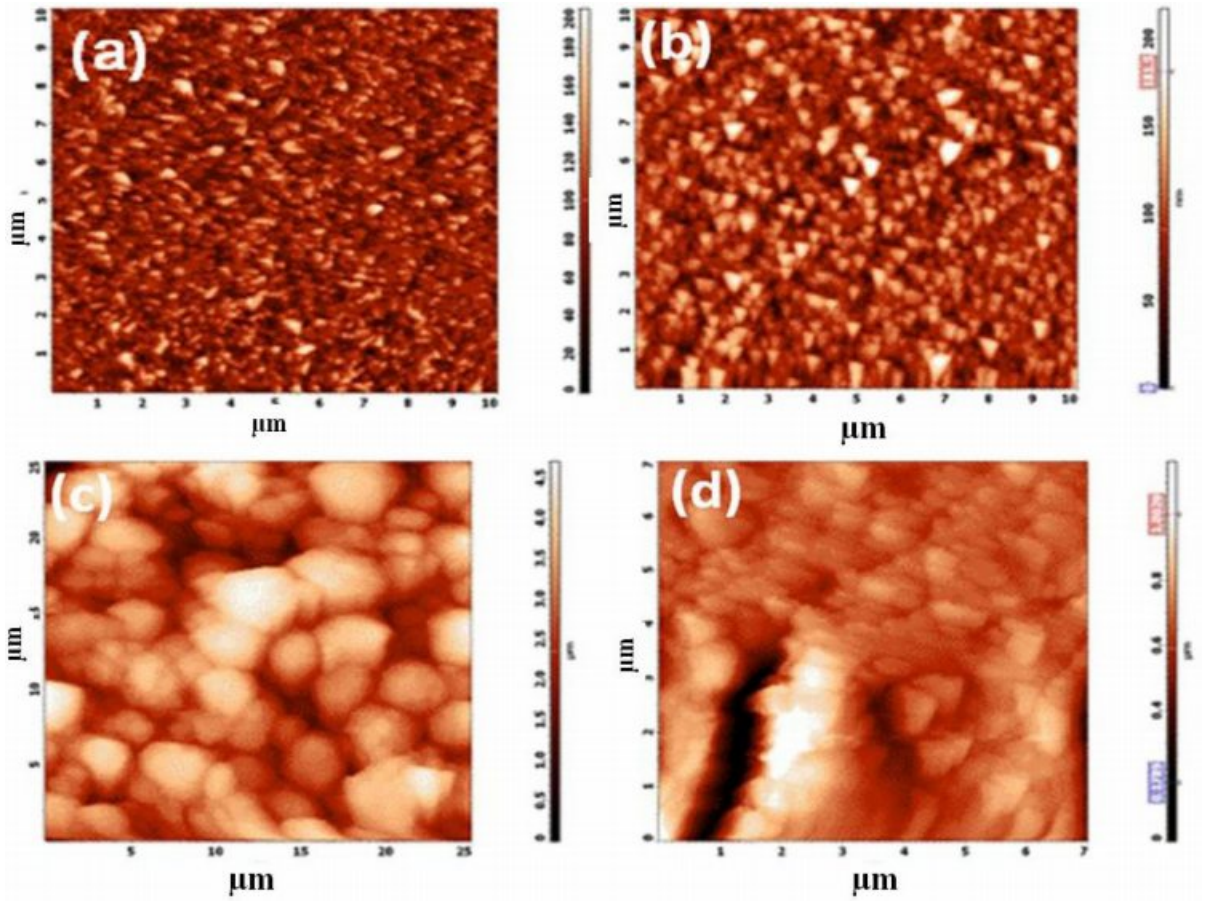

Fig. 2. AFM 2D - Images of (a) Bare FTO; (b) Compact Layer of Nanocrystalline TiO_2 (c) Active layer photoanode; (d) *(RuMOP-Pyz-1)* dye adsorbed on TiO_2 active layer respectively.

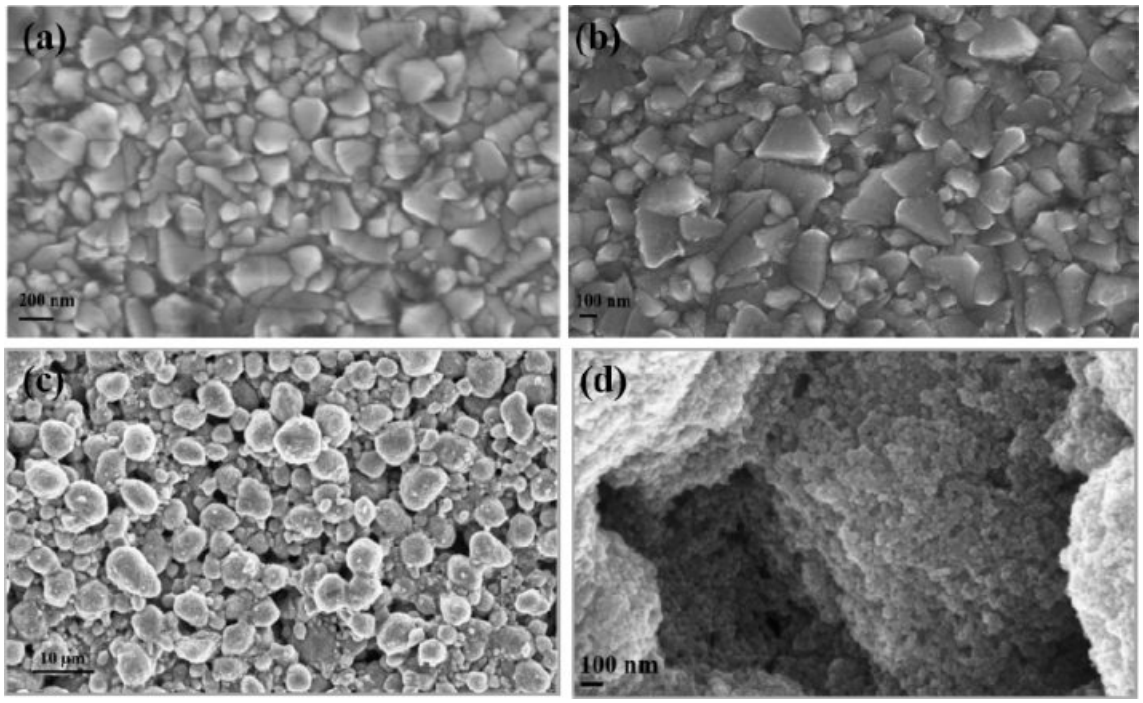

Fig. 3. FESEM Images of nanocrystalline TiO_2 photoanode (a) Bare FTO; (b) Compact Layer; (c) Active layer; (d) Porosity on TiO_2 active layer respectively.

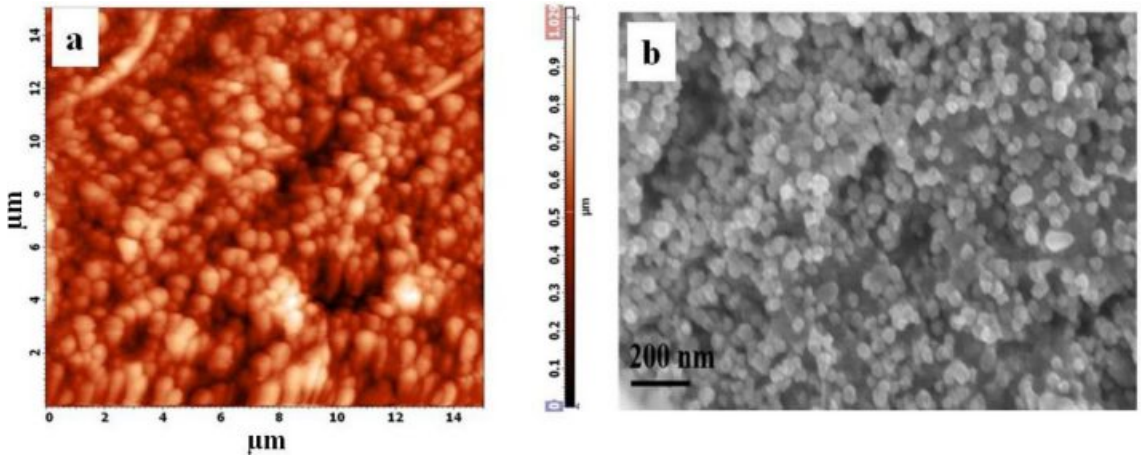

Fig. 4. (a) 2D AFM image and (b) FESEM image of platinum photocathode respectively.

steps. In Fig. 3(c) globular structures with aggregated nanoparticles were noted on the above of compact layer as TiO_2 photoanode. In particular, Fig. 3(d) depicts the availability of porosity for the deep penetration of the dye within TiO_2 was observed which enhances the easy electron transfer from LUMO of the dye to the HOMO of the TiO_2 nanoparticles. The available porosity in between the TiO_2 nanoparticles is very essential for the effective dye adsorption.

The photo cathode preparation and its corresponding AFM and FE-SEM images were given in Fig. 4(a & b) respectively. The AFM 2D image displays the uniform distribution of Pt nanoparticles on FTO. The high resolution image of the FESEM (Fig. 4b), provides information of the platinum electrode prepared by spray coating. The layer appears conformal with the conductive oxide surface and show good layer uniformity. Hence, we can see how the platinum nanoparticles are localized on the FTO surface. Importantly, the coated particle was interconnected continuously and produces highly porous structures of Pt nanoparicles.

I-V characteristics

The current density (J) versus voltage (V) curves of the DSSC is shown in Fig. 5. The photovoltaic measurements of open circuit voltage (V_{oc}), short circuit current density (J_{sc}), fill factor (FF), and the PCE (η) values were shown in Table 1. The DSSC

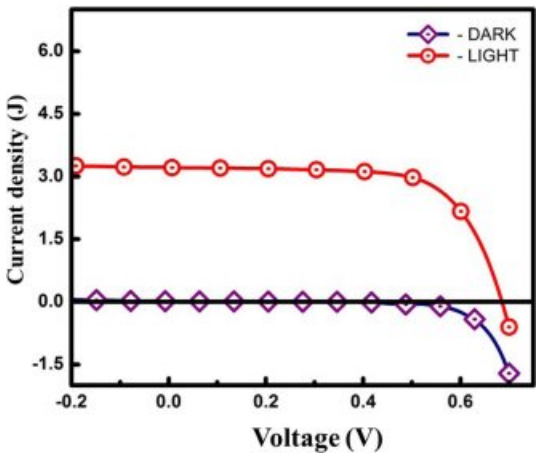

Fig. 5. Photovoltaic curve (J-V) measurements of fabricated DSSC device in which ***(RuMOP-Pyz-1)*** as sensitizer. (DARK - without sunlight, LIGHT - under Air Mass (AM) 1.5 G simulated sunlight at a light intensity of 100 mW/cm^2)

Table 1. Photovoltaic properties of fabricated DSSC device.

Dye	V_{oc} (V)	J_{sc} (mA/cm^2)	FF (%)	Efficiency (%)
RuMOP-Pyz-1	0.684	3.22	68.45	1.507

fabricated with the synthesized metal organic polymer *(RuMOP-Pyz-1)*, exhibited the photo conversion efficiency value (η) of 1.51% with short circuit current (J_{sc}) 3.22 mA/cm^2; open circuit voltage (V_{oc}) 0.684 V and Fill Factor (*FF)* 68.45%. When compared to the reported ruthenium dyes, 2,2'-bipyridine 4,4'-dicarboxylic acid based supramolecular ruthenium main-chain metal organic polymer which has pyrazine conjugated bridging ligand acting as linker unit, has better photovoltaic properties. By using linear ligands through the conjugated linker units, the charge separation distance and the charge recombination effects in DSSCs can be controlled. Normally, the carboxylic group in dcbpy moiety will be attached to the TiO_2 surface and thus by acting an electron withdrawing substituent in the bipyridine ligand. So, in this synthesized metal organic polymer which has more number of dicarboxylic acid group (dcbpy) throughout the polymer provides the necessary coupling of the LUMO level of dye with the conduction band of titanium dioxide, in order to promote efficient quantum injection.

Conclusions

In summary, $[Ru(II)(dcbpy)_2(pyz)]_n(BF_4)_{2n}$ based metal organic polymer *(RuMOP-Pyz-1)* was successfully synthesized and employed as a sensitizer in DSSC. The synthesized metal organic polymer was characterized using various spectroscopic and microscopic techniques. A maximum conversion efficiency of 1.51% with short circuit current (J_{sc}) 3.22 mA/cm^2; open circuit voltage (V_{oc}) 0.684 V and Fill Factor (FF) 68.45% under Air Mass (AM) 1.5 G simulated sunlight at a light intensity of 100 mW/cm^2 was obtained. The efficiency of the device and its photovoltaic performances were found to be satisfactory. The enhanced performance of the device is attributed to the presence of extended conjugation of the metallo polymer which helps in a facile electron transfer from the HOMO to LUMO of TiO_2. The results reported in this paper can provide new insights in improving the performance of DSSC in future.

Acknowledgements

The authors wish to acknowledge the facilities and support provided by PSG Sons & Charities Coimbatore, India.

References

1. B. O' Regan and M. Gratzel, Nature 353 (1991) 737-740.
2. M.K. Nazeeruddin, R. Splivallo, P. Liska, P. Comte, and M. Grätzel, Chem. Commun. 12 (2003) 1456-1457.
3. M. Grätzel, Accounts. Chem. Res. 42 (2009) 1788-1798.
4. J.B. Baxter, J. Vac. Sci. Tech. A. 30 (2012) 020801.
5. A. Hagfeldt, G. Boschloo, L. Sun, L. Kloo, and H. Pettersson, Chem. Rev. 110 (2010) 6595-6663.
6. T.L. Bahers, E. Brémond, I. Ciofini, and C. Adamo, Phys. Chem. Chem. Phys. 16 (2014) 14435-14444.
7. A.S. Polo, M.K. Itokazu, and N.Y.M. Iha, Coordin. Chem. Rev. 248 (2004) 1343-1361.
8. A. Yella, H-W. Lee, H.N. Tsao, C. Yi, A.K. Chandiran, M.K. Nazeeruddin, E. Diau, C.Y. Yeh, S.M. Zakeeruddin, and M. Gratzel, Science 334 (2011) 629-634.
9. A. Carella, F. Borbone, and R. Centore, Front. Chem. 6 (2018) 481.
10. J. Albero and P. Atienzar, A. Corma, H. Garcia, Chem. Rec. 15 (2015) 803-828.
11. J.N. Clifford, E. Martínez-Ferrero, A. Viterisi, and E. Palomares, Chem. Soc. Rev. 40 (2011) 1635-1646.
12. L. Loh and S. Dunn, J. Nanosci. Nanotechno. 12 (2012) 1-16.
13. W. Wunderlich, T. Oekermann, L. Miao, N.T. Hue, S. Tanemura, and M. Tanemura, J. Ceram. Process. Res. 5 [4] (2004) 343-354.
14. C.-P. Lee, K.-M. Lee, P.-Y Chen, and K.-C. Ho, Sol. Energ. Mat. Sol. C. 93 (2009) 1411-1416.
15. H.S. Chen, S.J. Lue, Y.L. Tung, K.W. Cheng, F.Y. Huang, and K.C. Ho, J. Power. Sources. 196 (2011) 4162-4172.
16. Liu, Yalin Lu, Z.B. Xie, and G.M. Chow, Sol. Energ. Mat. Sol. C. 95 (2011) 800-803.
17. G. Monros, M. Llusar, A. García, C. Gargori, and R. Galindo. Adv. Sci. Tech. 68 (2010) 182-193.
18. S.I. Noh, T-Y. Seong, and H-J. Ahn, J. Ceram. Process. Res. 13 [4] (2012) 491-494.
19. H. An, G-H. An, and H-J. Ahn, J. Ceram. Process. Res. 16 [2] (2015) 208-212.
20. S.I. Noh and H-J. Ahn, J. Ceram. Process. Res. 13 (2012) s1-s5.
21. W-S. Kwack, H-J. Choi, W-C. Choi, H-R Oh, S -Y Shin, K. Moon, J-Y Kwak, Y-K. Jeong, S-H. Kwon. J. Ceram. Process. Res. 13[3] (2012) 338-342.
22. H. Lee, J-I. Park, T-H. Kim, and K-B. Park. J. Ceram. Process. Res. 14[3] (2013) 405-409.

23. F. Shao, J. Sun, L. Gao, S. Yang, J. Luo. J. Phys. Chem. C 115[5] (2011) 1819-1823
24. L. Shi, X. Liu, H. Li, and G. Xu. Anal. Chem. 78 (2006) 7330-7334.
25. S.Y. Tsai, C.T. Ni, and K.Z. Fung. Ceram. Int. 43 (2017) S460-S463.
26. S. Ahmada, A.K. Pandey, N.A. Rahima, S. Shahabuddinb, and S.K. Tyagi Ceram. Int. 44[15] (2018) 18444-18449.
27. M.I. Khana, M.A. Rehman, M. Saleem, M.R. Baig, S. Rehman, W.A. Farooq, M. Atif, and A. Hanif, Ceram. Int. 45[16] (2019) 20589-20592.
28. T. Oku, S. Nagaoka, A. Suzuki, K. Kikuchi, Y. Hayashi, H. Sakuragi, and T. Soga, J. Ceram. Process. Res. 9[6] (2008) 549-552.
29. Y. Ren, D. Sun, Y. Cao, H.N. Tsao, Y. Yuan, S.M. Zakeeruddin, P. Wang, and M. Gratzel, J. Am. Chem. Soc. 140[7] (2018) 2405-2408.
30. N.A. Ludin, A.M. Mahmoud, A.B. Mohamad, A.A.H. Kadhum, K. Sopian, and N.S. Abdul Karim, Renew. Sust. Energ. Rev. 31 (2014) 386-396.
31. Y.S. Yen, H.H. Chou, Y.C. Chen, C.Y. Hsu, and J.T. Lin, J. Mater. Chem. 22 (2012) 8734-8747.
32. W.Y. Wong, J. Organomet. Chem. 694 (2009) 2644-2647.
33. N. Kakuta, T. Oku, A. Suzuki, K. Kikuchi, and S. Kikuchi, J. Ceram. Process. Res. 13[1] (2012) 28-31.
34. C.A. Bignozzi, R. Argazzi, R. Boaretto, E. Busatto, S. Carli, F. Ronconi, and S. Caramori, Coordin. Chem. Rev. 257 (2013) 1472-1492.
35. S. Sethi, S. Jena, P.K. Das, and N. Behera, J. Mol. Struc. 1193 (2019) 495-521.
36. S.S. Mali, C.A. Betty, P.N. Bhosale, and P.S. Patil, Electrochim. Acta. 59 (2012) 113-120.
37. C. Cai, S. Tseng, M. Kuo, K. Lin, H. Yang, and R. Lee RSC. Adv. 5 (2015) 102803-102810.
38. B. Nagarajan, S. Kushwaha, R. Elumalai, S. Mandal, K. Ramanujam, and D. Raghavachari, J. Mater. Chem. A. 5 (2017) 10289-10300.
39. T. Daeneke, T.H. Kwon, A. B. Holmes, N. W. Duffy, U. Bach, and L. Spiccia, Nat. Chem. 3 (2011) 211-215.
40. Q. Jiang, Z. Chu, P. Wang, X. Yang, H. Liu, Y. Wang, and J. You, Adv. Mater. 29 (2017) 1703852.
41. B. Hailegnaw, S. Kirmayer, E. Edri, G. Hodes, and D. Cahen, J. Phys. Chem. Lett. 6 (2015) 1543-1547.
42. P. Billen, E. Leccisi, S. Dastidar, S. Li, L. Lobaton, S. Spatari, and J. B. Baxter, Energy, 166 (2018) 1089-1096.
43. S. Yun, Y. Qin, A.R. Uhl, N. Vlachopoulos, M. Yin, D. Li, and A. Hagfeldt, Energy Environ. Sci. 11 (2018) 476-526.
44. R. Su, S. Ashraf, and A. El-Shafei, Sol. Energy 177 (2019) 724-736.
45. J.A. Cuello-Garibo, C.C. James, M.A. Siegler, and S. Bonnet, Eur. J. Inorg. Chem. 25 (2018) 1260-1268.
46. J.C. Salsman, S. Ronco, C.H. Londergan, and C.P. Kubiak, Inorg. Chem. 45 (2006) 547-554.
47. Q. Yu, S. Liu, M. Zhang, N. Cai, Y. Wang, and P. Wang, J. Phys. Chem. C 113 (2009) 14559-14566.
48. D. Bari, N. Wrachien, R. Tagliaferro, S. Penna, T.M. Brown, and A. Reale, A. Cester, Microelectron. Reliab. 51 (2011) 1762-1766.
49. A. Wild, A. Winter, and F. Schlütter, U. S. Schubert, Chem. Soc. Rev. 40 (2011) 1459-1511.
50. K. Feng, X. Shen, Y. Li, Y. He, D. Huang, and Q. Peng, Polym. Chem. 4 (2013) 5701-5710.
51. J. Xiang, C.L. Ho, and W.Y. Wong, Polym. Chem. 6 (2015) 6905-6930.
52. A.L.A. Parussulo, T.A. Matias, R.R. Guimaraes, S.H. Toma, K. Araki, and H.E. Toma, Inorg. Chim. Acta, 453 (2016) 764-770.
53. A.M.W.C. Thompson, M.C.C. Smailes, J.C. Jeffery, and M.D.J. Ward, J. Chem. Soc. Dalton Trans. (1997) 737-744.
54. M. Plevoets, F. Vögtle, L. De Cola, and V. Balzani, New J. Chem. 23 (1999) 63-69.
55. M.K. Nazeeruddin, S.M. Zakeeruddin R.H. Baker, M. Jirousek, P. Liska, N. Vlachopoulos, V. Shklover, C-H. Fischer, and M. Gratzel, Inorg. Chem. 38[26] (1999) 6298-6305.
56. C.A. Mitsopoulou, I. Veroni, A.I. Philippopoulos, and P. Falaras, J. Photoch. Photobio. A. 191 (2007) 6-12.